The Journal of Toxicological Sciences (J. Toxicol. Sci.)
Vol.38, No.3, ***-***, 2013

Toxicomics Report

Comparative gene expression analysis of the amygdala in autistic rat models produced by pre- and post-natal exposures to valproic acid

Atsuko Oguchi-Katayama[1], Akihiko Monma[2], Yuko Sekino[1], Toru Moriguchi[2] and Kaoru Sato[1]

[1]Laboratory of Neuropharmacology, Division of Pharmacology, National Institute of Health Sciences, 1-18-1 Kamiyoga, Setagaya-ku, Tokyo 158-8501, Japan
[2]Department of Food and Life Sciences, Azabu University, 1-17-71 Fuchinobe, Tyuoku, Sagamihara-shi, Kanagawa 252-5201, Japan

(Received October 24, 2012; Accepted March 14, 2013)

ABSTRACT — Gene expression profiles in the amygdala of juvenile rats were compared between the two autistic rat models for mechanistic insights into impaired social behavior and enhanced anxiety in autism. The rats exposed to VPA by intraperitoneal administration to their dams at embryonic day (E) 12 were used as a model for autism (E2IP), and those by subcutaneous administration at postnatal day (P) 14 (P14SC) were used as a model for regressive autism; both of the models show impaired social behavior and enhanced anxiety as symptoms. Gene expression profiles in the amygdala of the rats (E12IP and P14SC) were analyzed by microarray and compared to each other. Only two genes, Neu2 and Mt2a, showed significant changes in the same direction in both of the rat models, and there were little similarities in the overall gene expression profiles between them. It was considered that gene expression changes per se in the amygdala might be an important cause for impaired social behavior and enhanced anxiety, rather than expression changes of particular genes.

Key words: Valproic acid, Amygdala, Microarray, Prenatal, Postnatal

INTRODUCTION

There are two similar but different kinds of autistic animal models produced by perinatal exposure of rodents to valproic acid (VPA). Rodents exposed to VPA on embryonic day (E) 12 have been used as an animal model for autism characterized by impaired social behavior, enhanced anxiety, and decreased sensitivity to pain after maturation (Markram *et al.*, 2008; Schneider and Przewtocki, 2005; Schneider *et al.*, 2007, 2008). On the other hand, rodents exposed to VPA on postnatal day (P) 14 have been used as an animal model for regressive autism that shows impaired social behavior like animal models for autism but accompanied by loss of some acquired skills (Yochum *et al.*, 2008, 2010; Wagner *et al.*, 2006). The regressive autism model also showed enhanced anxiety in our preliminary study.

The amygdala has been considered critical for behaviors associated with emotional disorders. Possible mechanisms of impaired social behavior in autism involve neural networks including the amygdala (Neuhaus *et al.*, 2010). The amygdala has also been identified to be involved in anxiety behaviors (Blackford and Pine, 2012). In humans, the amygdala and prefrontal cortex is the responsible for anxiety disorders (Etkin and Wager, 2007). It is therefore expected that comparative analysis of the amygdala in the two animal models for autism provide some mechanistic insights into impaired social behavior and enhanced anxiety in autism from similarities between them.

In the present study, we performed comparative gene expression analysis of the amygdala and characterize the similarities between the animal models for autism and for regressive autism. We first confirmed the effect of postnatal exposure to VPA on anxiety-related behavior in rats. We then compared gene expression profiles in the amygdala of juvenile rats between prenatal and postnatal exposures to VPA.

Correspondence: Kaoru Sato (E-mail: kasato@nihs.go.jp)

MATERIALS AND METHODS

Animals and VPA treatment

Pregnant Wistar Hannover/Rcc rats were obtained from Japan SLC, Inc. (Shizuoka, Japan) and maintained individually under conventional conditions with controlled temperature (23 ± 3°C) and illumination (12 hr; 7:00-19:00). Each of five litters was culled to 10 pups/litter on day 2 after birth for matched nursing conditions. For postnatal exposure, saline or 400 mg/kg of VPA (Sigma, St. Louis, MO, USA) was administered subcutaneously (s.c.) to half of the pups in each litter on postnatal day 14 (P14SC). For prenatal exposure, saline or 600 mg/kg of VPA was administered intraperitoneally (i.p.) to five pregnant rats on E12 (E12IP). Microarray analysis was performed at 5 (E12IP and P14SC) or 7 (P14SC7w) wks after the VPA administrations (Fig. 1). All animal treatments and experimental protocols were approved by the Animal Care and Use Committee of the Azabu University and the National Institute of Health Science (NIHS), and followed the Guide for the Care and Use of Laboratory Animals.

Behavioral test for anxiety

As a behavioral test, elevated plus maze (EPM) was performed in P14SC at 5 wks old with a maze consists of two opposite open arms (50 × 10 cm) and two opposite enclosed arms. The arms are connected by a central 10-cm square, forming a plus shape. The maze was elevated 50 cm above the floor. The animal's path was observed for 5 min after a resting period of 2 min in the central square of the maze. The number of entries into the open arms and the time spent in the open arms were measured.

Microarray analysis

Microarray analysis was performed using animals different from those used for behavioral test. The amygdalae were removed from the juvenile rats, and incubated in a RNA stabilization solution (RNAlater, Ambion, Austin, TX, USA) (1 ml for 5 x 5 x 5 (mm) block) overnight. Total RNA samples from the amygdalae were isolated with TRIzol (Invitrogen, Carlsbad, CA, USA) and the RNeasy Mini Kit (Qiagen, Hilden, Germany), with slight modifications to the manufacturer's protocol. The

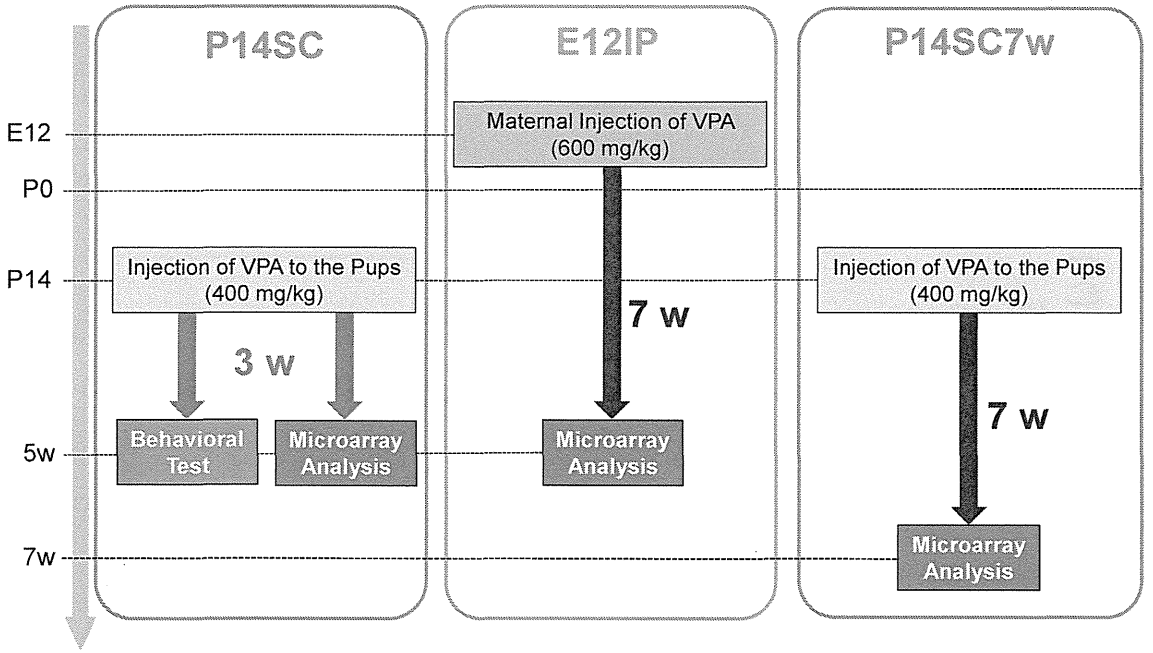

Fig. 1. The experimental design. To investigate the effect of postnatal VPA exposure on behavior and gene expression profiles, saline or 400 mg/kg VPA was administered to half of the pups per one litter subcutaneously on postnatal day 14 (P14SC). Behavior test and microarray analysis were performed using individual animals. To avoid influence of the dams, 5w juvenile rats (P35-37) were obtained evenly from 5 litters for control group and VPA- treated group, respectively. To investigate the effect of prenatal exposure, five pregnant rats were treated intraperitoneally (i.p.) with saline or 600 mg/kg VPA on E12.5 (E12IP), respectively, and microarray analysis was performed at 5w (P35-37). To analyze the contribution of the length of time from VPA exposure to cRNA isolation to the change in gene expression profile, microarray analysis was also performed at 7w (P49-56) (5 w after VPA exposure at P14) (P14SC7w).

isolated RNA sample (100 μg) were used for the microarray analysis (Affymetrix GeneChip Rat Genome 230 2.0 array (Santa Clara, CA, USA)) according to the Affymetrix protocol (http://www.affymetrix.com/support/technical/manuals.affx). Data were collected using Affymetrix GeneChip® Operating Software (GCOS) (http://media.affymetrix.com/support/technical/whitepapers/sadd_whitepaper.pdf).

Data analysis

Data analyses were carried out with GeneSpring (Agilent Technologies, Santa Clara, CA, USA). All of the data from the VPA-treated groups were normalized to the median of the control groups, and the expression of each selected gene was calculated as a log ratio of the signal to the control value. To assess the differences between the control and VPA-treated groups, the Benjamini and Hochberg false-discovery rate (FDR) method was employed, and those with a p-value less than 0.05 were considered as significant. Network, function, and pathway analyses were performed using Ingenuity Pathway Analysis software (IPA; Ingenuity Systems, Redwood City, CA, USA).

RESULTS AND DISCUSSION

Behavioral tests for anxiety

The time spent in the open arms was significantly shorter in the males of P14SC than in those of the corresponding control, indicating enhanced anxiety by postnatal exposure to VPA (Fig. 2, left). There were, however, no significant changes in the behavior test of the females (Fig. 2, right). There were no effects of the VPA exposure on the number of entries into the open arms in both genders (data not shown). These results indicate that postnatal exposure to VPA caused enhanced anxiety specifically in males. This sexual dimorphism is a typical feature of autism and has been observed in the animal model for autism produced by prenatal exposure to VPA (Schneider *et al.*, 2008). We therefore analyzed the gene expression profile of the amygdala exposed to VPA only in males in the following experiments.

Gene expression microarray analysis

In the controls, gene expression profiles were almost identical among the varied VPA exposure conditions. The number of genes with expression levels different from those in the corresponding controls was larger in P14SC (53 probe sets for 49 genes) than in E12IP (32 probe sets for 30 genes), excluding expressed sequence tags (Fig. 3A). Functional classification of the genes also indicated the differences of gene expression between P12IP and P14SC (Fig. 3B). P14SC contained a wider variety of categories than E12IP; 'phosphatase' appeared only in E12IP, while 'cytokine', 'growth factor', 'lig-

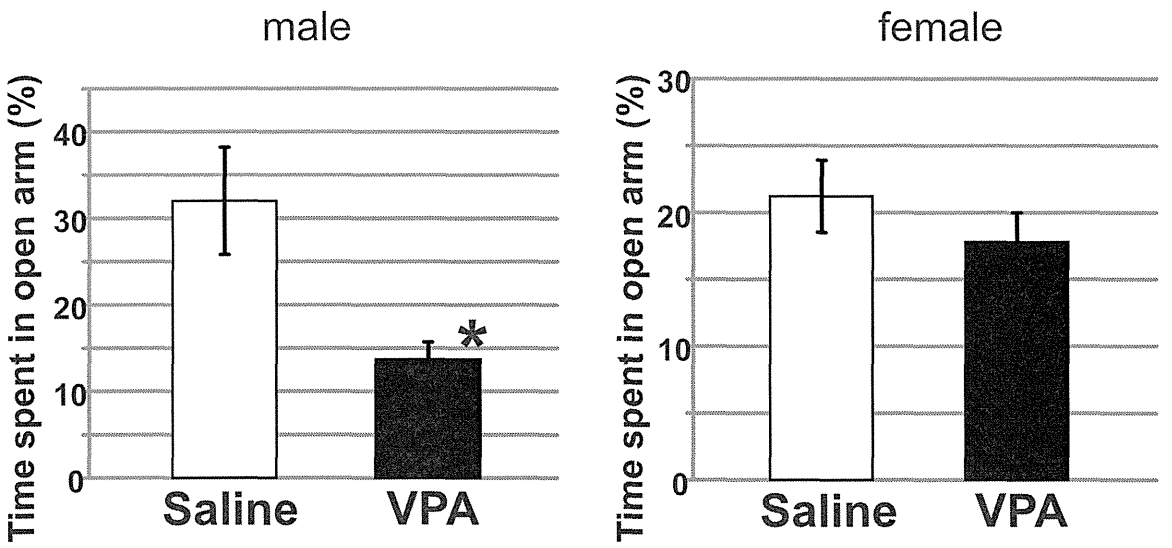

Fig. 2. The effects of postnatal exposure to VPA on anxiety-related behavior. 400 mg/kg VPA was administered to animals subcutaneously at P14. Anxiety-related behaviors were analyzed at 5w by EPM. Total open arm entries and time spent in open arm are quantified. The data of time spent in open arm were shown. An asterisk indicates a statistically significant difference from the control ($P < 0.05$, $N = 13$-15, Student's t test).

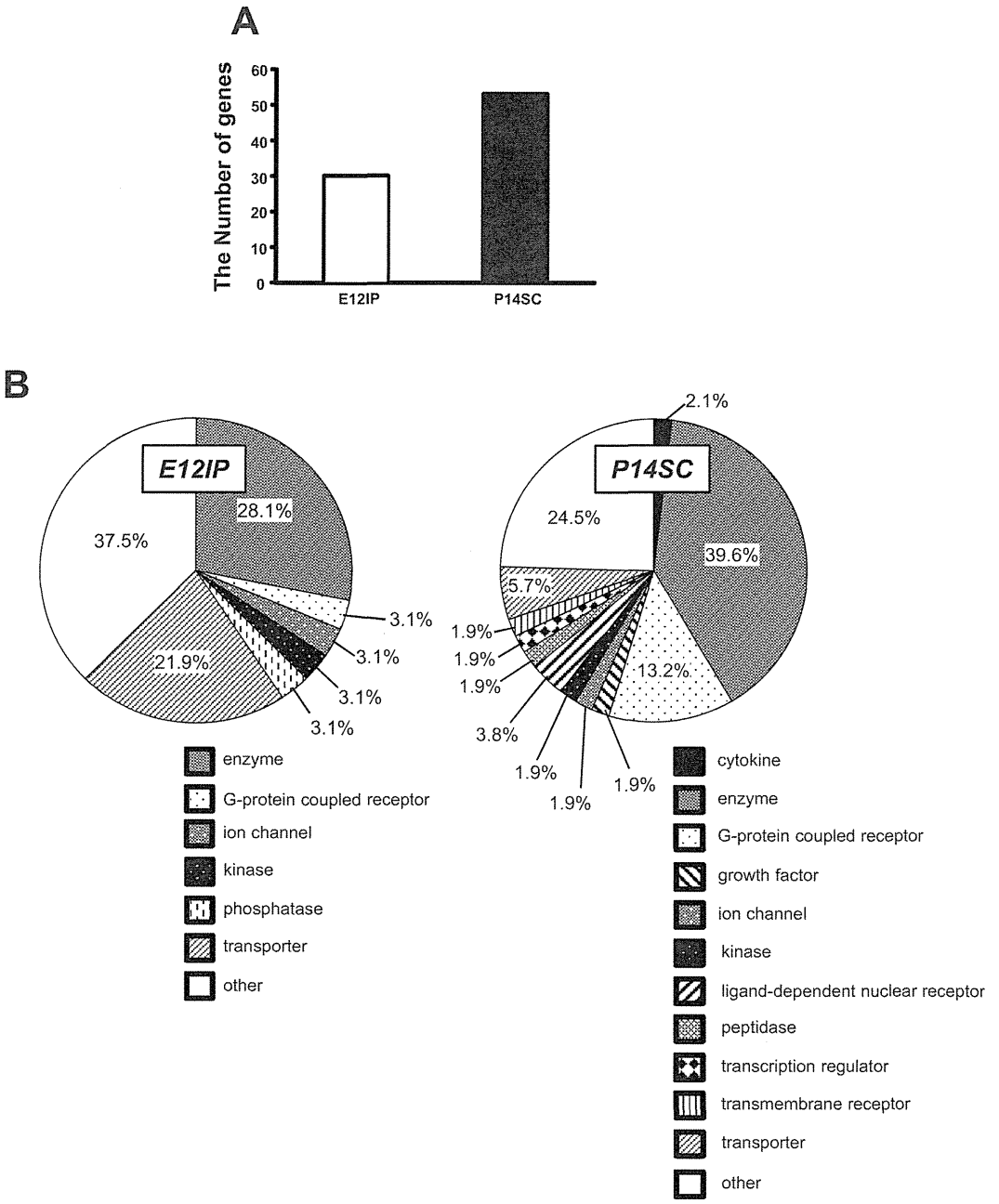

Fig. 3. Summary of the gene expression profiles of E12IP and P14SC rats (male). For both of E12IP and P14SC, total RNA of the amygdalae of 5w male rats (P33-37, N = 4) were analyzed with the microarray chip. Data were collected using Affymetrix GeneChip® Operating Software (GCOS) and analyzed using GeneSpring software. A. The numbers of significantly changed genes in E12IP and P14SC ($p < 0.05$, N = 4). B. Functional classification of the significantly changed genes by GeneSpring.

and-dependent nuclear receptor', 'peptidase', 'transcription regulator', and 'transmembrane receptor' appeared only in P14SC. As for categories common to E12IP and P14SC, their proportions were different from each other; e.g., 'transporters' accounted for 21.9% in E12IP but only 5.7% in P14SC.

Only two genes, Neu2 and Mt2a, exhibited the significant changes in the same direction in E12IP and P14SC

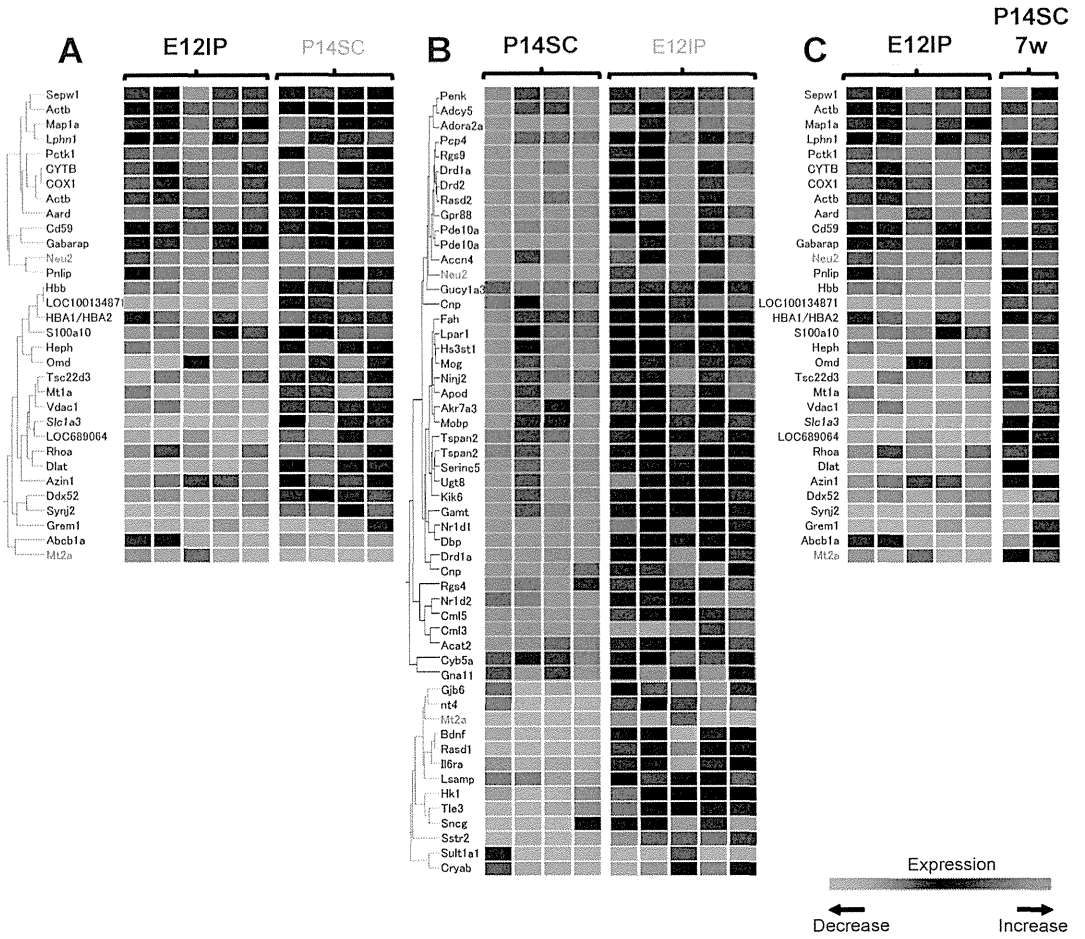

Fig. 4. Heat maps representing hierarchical clustering of the significantly changed genes of E12IP and P14SC. Each vertical column represents an individual sample, and each horizontal row represents a single gene. (N = 4 for P14SC and E12IP, N = 2 for P14SC7w) A. A heat map/hierarchical clustering of the significantly changed genes of E12IP with a heat map of the same genes of P14SC. Clustering was performed using the Benjamini and Hochberg FDR method. B. A heat map/hierarchical clustering of the significantly changed genes of P14SC with a heat map of the same genes of E12IP. C. A heat map of E12IP was compared with that of P14SC7w in which cRNA was extracted 7 w after VPA exposure at P14.

(red letters in Figs. 4A and B). The expression profile in E12IP was also different from that in P14SC7w (Fig. 4C), suggesting that the differences between E12IP and P14SC were not due to the varied length of time between the VPA exposure and the gene expression analysis. Precise gene lists for the heat maps of E12IP (Fig. 4A) and P14SC (Fig. 4B) are shown in Table 1 and Table 2, respectively. 'Behavior'-related genes were identified only in P14SC (Table 3). A larger number of genes were categorized as 'nervous system development and function', 'neurological disease' and 'psychological disorders' in P14SC than in E12IP.

Pathway analysis

The most significantly changed network (Fig. 5A [i]) was that linking 'cell death', 'cellular compromise', and 'neurological disease'. The hubs of this network were MYC, HTT, and CASP3, although the expression levels of these three genes remained unchanged. The second most significantly changed network was that linking 'cell death', 'neurological disease', and 'carbohydrate metabolism' (Fig. 5A [ii]). TNF, which plays an especially important role in cell death, was a highly interconnected node. In P14SC, three significant networks were identified (Fig. 5B [i]-[iii]). These networks are related to 'nucleic acid metabolism' (Fig. 5B [i]), 'cell signaling' (Fig. 5B

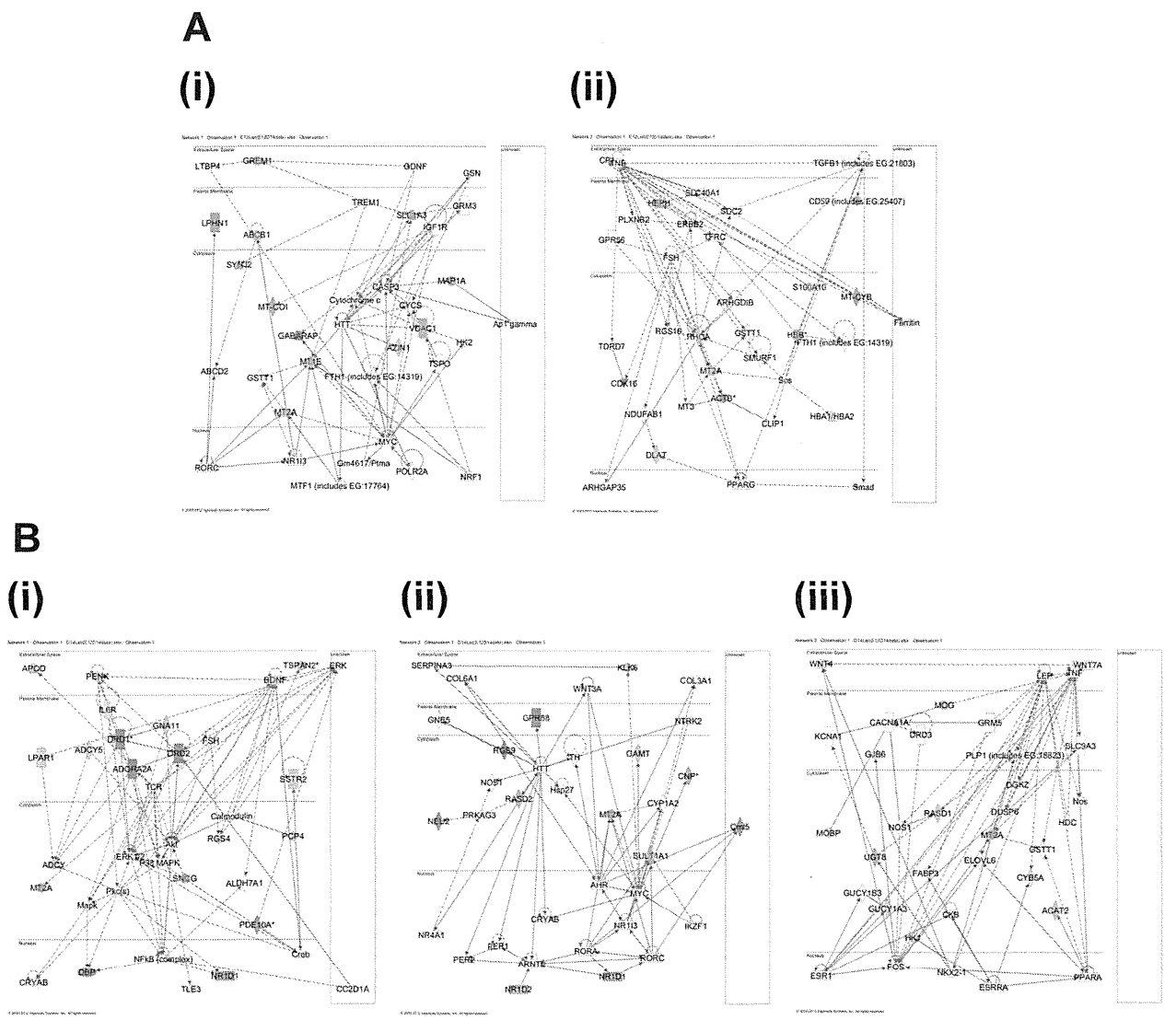

Fig. 5. IPA networks generated with significantly changed genes of E12IP and P14SC. A. The first (i) and second (ii) most significantly altered networks in E12IP. The most significantly changed network linked 'cell death', 'cellular compromise', and 'neurological disease'. The second most significantly changed network linked 'cell death', 'neurological disease', and 'carbohydrate metabolism'. B. The first (i), second (ii), and third (iii) most significantly changed networks in P14SC. These networks are related to 'nucleic acid metabolism' (i), 'cell signaling' (ii), and 'neurological disease' (iii).

[ii]), and 'neurological disease' (Fig. 5B [iii]). One notable aspect of these networks that was not observed in the E12IP networks is the alterations in the expression levels of nuclear genes such as DBP (transcription regulator), NR1D1 (nuclear receptor), and NR1D2 (nuclear receptor).

In conclusion, there are little similarities in the gene expression profiles between the two rat models for autism and regressive autism produced by pre- and post-natal exposures to VPA respectively. It is considered that that gene expression changes per se in the amygdala may be an important cause for impaired social behavior and enhanced anxiety, rather than expression changes of particular genes.

Table 1. The list of genes which changed significantly in E12IP

ID	Symbol	Entrez Gene name	Type(s)
Increase			
1389956_a_at	MT-COI	cytochrome c oxidase subunit I	enzyme
1367996_a_at	LPHN1	latrophilin 1	G-protein coupled receptor
1367882_at	MAP1A	microtubule-associated protein 1A	other
1388159_at	MT-CYB	cytochrome b	enzyme
1367929_at	CD59 (includes EG:25407)	CD59 molecule, complement regulatory protein	other
1398836_s_at	ACTB	actin, beta	other
1368127_at	NEU2	sialidase 2 (cytosolic sialidase)	enzyme
1398835_at	ACTB	actin, beta	other
1370326_at	CDK16	cyclin-dependent kinase 16	kinase
1370804_at	GABARAP	GABA(A) receptor-associated protein	transporter
1367593_at	SEPW1	selenoprotein W, 1	enzyme
1368554_at	PNLIP	pancreatic lipase	enzyme
1370459_at	C8orf85	chromosome 8 open reading frame 85	other
Decrease			
1387197_at	OMD	osteomodulin	other
1371245_a_at	HBB	hemoglobin, beta	transporter
1371130_at	SLC1A3	solute carrier family 1 (glial high affinity glutamate transporter), member 3	transporter
1368971_a_at	SYNJ2	synaptojanin 2	phosphatase
1371102_x_at	LOC100134871	beta globin minor gene	other
1369113_at	GREM1	gremlin 1	other
1371237_a_at	MT1E	metallothionein 1E	other
1368533_at	HEPH	hephaestin	transporter
1368588_at	DDX52	DEAD (Asp-Glu-Ala-Asp) box polypeptide 52	enzyme
1367771_at	Tsc22d3	TSC22 domain family, member 3	other
1386909_a_at	VDAC1	voltage-dependent anion channel 1	ion channel
1388271_at	MT2A	metallothionein 2A	other
1370464_at	ABCB1	ATP-binding cassette, sub-family B (MDR/TAP), member 1	transporter
1367553_x_at	HBB	hemoglobin, beta	transporter
1386890_at	S100A10	S100 calcium binding protein A10	other
1370575_a_at	AZIN1	antizyme inhibitor 1	enzyme
1370130_at	RHOA	ras homolog gene family, member A	enzyme
1388194_at	DLAT	dihydrolipoamide S-acetyltransferase	enzyme
1388608_x_at	HBA1/HBA2	hemoglobin, alpha 1	transporter

ID, symbol, entrez gene name, type of each gene were shown based on IPA software database.

Table 2. The list of genes which changed significantly in P14SC

ID	Symbol	Entrez Gene name	Type(s)
Increase			
1386904_a_at	CYB5A	cytochrome b5 type A (microsomal)	enzyme
1387897_at	CNP	2',3'-cyclic nucleotide 3' phosphodiesterase	enzyme
1370048_at	LPAR1	lysophosphatidic acid receptor 1	G-protein coupled receptor
1368092_at	FAH	fumarylacetoacetate hydrolase (fumarylacetoacetase)	enzyme
1368506_at	RGS4	regulator of G-protein signaling 4	other
1368298_at	ADCY5	adenylate cyclase 5	enzyme
1370834_at	HS3ST1	heparan sulfate (glucosamine) 3-O-sulfotransferase 1	enzyme
1368154_at	GUCY1A3	guanylate cyclase 1, soluble, alpha 3	enzyme
1368145_at	PCP4	Purkinje cell protein 4	other
1368253_at	GAMT	guanidinoacetate N-methyltransferase	enzyme
1387822_at	GNA11	guanine nucleotide binding protein (G protein), alpha 11 (Gq class)	enzyme
1368263_a_at	MOBP	myelin-associated oligodendrocyte basic protein	other
1367949_at	PENK	proenkephalin	other
1370206_at	ACCN4	amiloride-sensitive cation channel 4, pituitary	ion channel
1386979_at	SERINC5	serine incorporator 5	transporter
1368104_at	TSPAN2	tetraspanin 2	other
1372462_at	ACAT2	acetyl-CoA acetyltransferase 2	enzyme
1398257_at	MOG	myelin oligodendrocyte glycoprotein	other
1398258_at	APOD	apolipoprotein D	transporter
1368105_at	TSPAN2	tetraspanin 2	other
1368384_at	KLK6	kallikrein-related peptidase 6	peptidase
1370541_at	NR1D2	nuclear receptor subfamily 1, group D, member 2	ligand-dependent nuclear receptor
1370693_a_at	CNP	2',3'-cyclic nucleotide 3' phosphodiesterase	enzyme
1368121_at	AKR7A3	aldo-keto reductase family 7, member A3 (aflatoxin aldehyde reductase)	enzyme
1368438_at	PDE10A	phosphodiesterase 10A	enzyme
1368858_at	UGT8	UDP glycosyltransferase 8	enzyme
1370372_at	RASD2	RASD family, member 2	enzyme
1370816_at	NR1D1	nuclear receptor subfamily 1, group D, member 1	ligand-dependent nuclear receptor
1368478_at	DRD1	dopamine receptor D1	G-protein coupled receptor
1370669_a_at	PDE10A	phosphodiesterase 10A	enzyme
1387874_at	DBP	D site of albumin promoter (albumin D-box) binding protein	transcription regulator
1388176_at	Cml5	camello-like 5	enzyme
1368135_at	NINJ2	ninjurin 2	other
1368127_at	NEU2	sialidase 2 (cytosolic sialidase)	enzyme
1368479_at	DRD1	dopamine receptor D1	G-protein coupled receptor

Table 2. (Continued)

ID	Symbol	Entrez Gene name	Type(s)
Increase			
1387241_at	GPR88	G protein-coupled receptor 88	G-protein coupled receptor
1368708_a_at	DRD2	dopamine receptor D2	G-protein coupled receptor
1368300_at	ADPRA2A	adenosine A2a receptor	G-protein coupled receptor
1368500_a_at	RGS9	regulator of G-protein signaling 9	enzyme
1370991_at	Cml3/Gm4477	camello-like 3	enzyme
Decrease			
1370550_at	LSAMP	limbic system-associated membrane protein	other
1370026_at	CRYAB	crystallin, alpha B	other
1386987_at	IL6R	interleukin 6 receptor	transmembrane receptor
1368641_at	WNT4	wingless-like MMTV integration site family, member 4	cytokine
1387169_at	TLE3	transducin-like enhancer of split 3 (E(sp 1) homolog, Drosophila)	other
1368577_at	GJB6	gap junction protein, beta 6, 30kDa	transporter
1386929_at	HK1	hexokinase 1	kinase
1368782_at	SSTR2	somatostatin receptor 2	G-proein coupled receptor
1368677_at	BDNF	brain-derived neurotrophic factor	growth factor
1387908_at	RASD1	RAS, dexamethasone-induced 1	enzyme
1370019_at	SULT1A1	sulfotransferase family, cytosolic, 1A, phenol-preferring, member 1	enzyme
1398245_at	SNCG	synuclein, gamma (breast cancer-specific protein 1)	other
1388271_at	MT2A	metallothionein 2A	other

ID, symbol, entrez gene name, type of each gene were shown based on IPA software database.

Table 3. The list of genes which changed significantly in E12IP and P14SC were categorized to groups based on their functions using IPA software

E12IP			P14SC	
p-value	Molecules	Category	P14SC	p-value
		Behavior	RGS9,GJB6,RASD2,DBP,BDNF,PDE10A,IL6R,CNP,SNCG,DRD2,PCP4,DRD1,NR1D1,LPAR1,ADCY5,PENK,ADORA2A	2.16E-07-1.85E-02
1.02E-02-1.02E-02	RHOA	Cell Cycle	CRYAB,SSTR2,WNT4	4.65E-03-1.85E-02
6.33E-06-3.04E-02	ABCB1,CD59,MT2A,RHOA,ACTB,GREM1,VDAC1,MT1E	Cell Death	CRYAB,BDNF,IL6R,RGS4,UGT8,DRD2,HK1,LPAR1,SSTR2,ADCY5,MT2A,ADORA2A,MOG	3.03E-04-2.31E-02
2.56E-03-4.46E-02	CD59,HBB,MT2A,RHOA,SLC1A3,VDAC1	Cell Morphology	HK1,LPAR1,DRD1,MT2A,BDNF,IL6R,GNA11,KLK6,RGS4,SNCG,DRD2,ADORA2A	4.59E-04-2.31E-02
4.93E-02-4.93E-02	CD59,HBA1/HBA2,VDAC1	Cell Signaling	RGS9,LPAR1,SSTR2,DRD1,BDNF,ADCY5,PDE10A,IL6R,GNA11,RGS4,DRD2,ADORA2A	9.12E-05-2.07E-02
6.3E-05-2.54E-02	CD59,MT2A,RHOA,SLC1A3,GREM1,GABARAP,VDAC1,LPHN1,MT1E,S100A10	Cell-To-Cell Signaling and Interaction	RASD2,GUCY1A3,BDNF,GNA11,CNP,IL6R,RGS4,KLK6,SNCG,DRD2,PCP4,DRD1,ADCY5,MT2A,SULT1A1,PENK,ADORA2A,MOG,NINJ2	2.34E-07-2.31E-02
6.33E-06-4.27E-02	SYNJ2,CD59,MT2A,RHOA,HBA1/HBA2,VDAC1,LPHN1,MT1E	Cellular Assembly and Organization	RGS9,HK1,CRYAB,LPAR1,DRD1,MT2A,BDNF,GNA11,CNP,SNCG,DRD2,MOG	4.65E-03-2.31E-02
4.67E-04-4.46E-02	Tsc22d3,HBB,MT2A,RHOA,HBA1/HBA2,SLC1A3,	Cellular Development	NR1D1,DRD1,MT2A,BDNF,SERINC5,IL6R,RGS4,UGT8,DRD2	5.55E-04-2.31E-02
1.32E-04-4.27E-02	CD59,MT2A,RHOA,HBA1/HBA2,VDAC1,LPHN1,MT1E	Cellular Function and Maintenance	CRYAB,DRD1,BDNF,CNP	4.65E-03-2.31E-02
4.67E-04-2.07E-02	ABCB1,MT2A,RHOA,ACTB,GREM1,GABARAP,VDAC1,MT1E	Cellular Growth and Proliferation	GJB6,CRYAB,GUCY1A3,BDNF,IL6R,GNA11,KLK6,RGS4,SNCG,DRD2,RASD1,SSTR2,LPAR1,NR1D1,MT2A,PENK,WNT4,ADORA2A,MOG	3.03E-04-2.17E-02
2.56E-03-4.77E-02	CD59,RHOA,LPHN1,S100A10	Cellular Movement	GUCY1A3,BDNF,GNA11,CNP,IL6R,RGS4,KLK6,SNCG,DRD2,NR1D1,SSTR2,DRD1,LPAR1,PENK,ADORA2A,MOG	6.76E-05-1.85E-02
1.67E-05-2.54E-02	Tsc22d3,MT2A,RHOA,GREM1,VDAC1,MT1E	Connective Tissue Development and Function		
5.12E-03-4.27E-02	HBB,RHOA,PNLIP	Developmental Disorder	CRYAB,GJB6,SSTR2,DRD1,GUCY1A3,BDNF,IL6R,GNA11,WNT4,RGS4,DRD2	2.02E-05-2.31E-02
7.67E-03-7.67E-03	ABCB1	DNA Replication, Recombination, and Repair	GUCY1A3,BDNF,RGS4,DRD2,ADORA2A	1.28E-02-1.28E-02
2.56E-03-4.27E-02	ABCB1	Drug Metabolism	DRD1,BDNF,SULT1A1,GNA11,RGS4,SNCG,DRD2,ADORA2A	2.12E-05-1.85E-02
2.56E-03-4.77E-02	HBB,RHOA,GREM1	Embryonic Development	GJB6,LPAR1,BDNF,WNT4,KLK6,DRD2	1.17E-03-1.85E-02
2.56E-03-2.56E-03	ABCB1	Endocrine System Development and Function	BDNF,SULT1A1,GNA11,WNT4,ADORA2A	2.1E-04-2.31E-02
2.25E-02-2.25E-02	MT1E,S100A10	Endocrine System Disorders	ACAT2,SSTR2,DRD1,IL6R,DRD2	2.02E-05-2.31E-02
4.52E-02-4.52E-02	RHOA	Gene Expression	DBP,BDNF,IL6R,RGS4,KLK6,NR1D2,DRD2,RASD1,NR1D1,DRD1,LPAR1,TLE3,WNT4,ADORA2A,MOG	1.38E-02-1.39E-02

Table 3. (Continued)

E12IP			P14SC	
p-value	Molecules	Category	P14SC	p-value
1.29E-03-4.27E-02	ABCB1,HBB,MT2A,ACTB,PNLIP,MT1E	Genetic Disorder	ACCN4,RGS9,CRYAB,GJB6,RASD2,ACAT2,BDNF,GNA11,KLK6,NR1D2,DRD1,ADCY5,MT2A,WNT4,LSAMP,MOG,GUCY1A3,DBP,PDE10A,CNP,IL6R,TSPAN2,RGS4,NEU2,SNCG,DRD2,GPR88,FAH,PCP4,LPAR1,NR1D1,MOBP,SSTR2,SULT1A1,PENK,TLE3,CYB5A,ADORA2A,APOD	4.1E-09-2.31E-02
2.56E-03-4.27E-02	ABCB1,RHOA,MT1E	Inflammatory Disease	CRYAB,BDNF,IL6R,DRD2,MOG	4.65E-03-2.31E-02
2.56E-03-4.27E-02	CD59,RHOA,MT1E,S100A10	Inflammatory Response	GNA11,IL6R,PENK,CNP,ADORA2A,MOG	9.29E-03-2.31E-02
2.56E-03-4.4E-02	SYNJ2,ABCB1,MT2A,DLAT,RHOA,MT1E,PNLIP,S100A10	Lipid Metabolism	ACAT2,DBP,BDNF,SERINC5,GNA11,RGS4,UGT8,DRD2,LPAR1,DRD1,SSTR2,SULT1A1,WNT4,ADORA2A,MOG,APOD	2.1E-04-2.31E-02
6.33E-06-4.93E-02	ABCB1,CD59,HBA1/HBA2,CDK16,SLC1A3,HEPH,LPHN1,HBB,MT-CYB,MT2A,RHOA,GABARAP,VDAC1,MT1E,PNLIP,S100A10	Molecular Transport	ACAT2,GUCY1A3,BDNF,PDE10A,GNA11,IL6R,RGS4,UGT8,SNCG,DRD2,HK1,LPAR1,SSTR2,DRD1,MT2A,ADCY5,WNT4,ADORA2A,APOD	1.11E-05-2.31E-02
3.99E-03-4.27E-02	MT2A,RHOA,HBA1/HBA2,SLC1A3,GABARAP,VDAC1,LPHN1,MT1E	Nervous System Development and Function	GJB6,RASD2,GUCY1A3,DBP,BDNF,SERINC5,CNP,GNA11,RGS4,UGT8,SNCG,DRD2,PCP4,DRD1,NR1D1,LPAR1,ADCY5,MT2A,PENK,ADORA2A,MOG,NINJ2	1.59E-05-2.31E-02
3.79E-05-3.78E-02	MT2A,ACTB,SLC1A3,MT1E,S100A10	Neurological Disease	RGS9,CRYAB,RASD2,GJB6,BDNF,GNA11,DRD1,MT2A,ADCY5,LSAMP,MOG,GUCY1A3,DBP,PDE10A,CNP,IL6R,RGS4,SNCG,DRD2,GPR88,PCP4,LPAR1,MOBP,SSTR2,NR1D1,PENK,ADORA2A,APOD	1.43E-09-2.31E-02
2.64E-02-2.64E-02	MT2A,MT1E	Psychological Disorders	CRYAB,BDNF,PDE10A,CNP,RGS4,DRD2,PCP4,MOBP,DRD1,SSTR2,MT2A,LSAMP,ADORA2A,MOG,APOD	1.57E-04-2.01E-02
6.33E-06-4.4E-02	ABCB1,AZIN1,HBA1/HBA2,SLC1A3,SYNJ2,HBB,MT2A,RHOA,DLAT,VDAC1,PNLIP,MT1E,S100A10	Small Molecule Biochemistry	RGS9,ACAT2,BDNF,SERINC5,GNA11,HK1,DRD1,MT2A,ADCY5,WNT4,MOG,DBP,GUCY1A3,PDE10A,IL6R,RGS4,UGT8,SNCG,DRD2,SSTR2,LPAR1,GAMT,SULT1A1,CYB5A,ADORA2A,APOD	1.11E-05-2.31E-02
2.56E-03-2.79E-02	CD59,Tsc22d3,HBB,RHOA,SLC1A3,GREM1	Tissue Development	GJB6,CRYAB,GUCY1A3,BDNF,GNA11,CNP,IL6R,KLK6,RGS4,DRD2,GAMT,DRD1,LPAR1,TLE3,WNT4,ADORA2A,MOG,NINJ2	4.59E-04-2.31E-02
3.43E-04-2.79E-02	CD59,HBB,MT2A,RHOA,SLC1A3,GREM1,MT1E,S100A10	Tissue Morphology	CRYAB,ACAT2,GUCY1A3,BDNF,IL6R,DRD2,GAMT,DRD1,SSTR2,LPAR1,WNT4,ADORA2A,MOG	8E-04-2.31E-02

Behavior'-related genes were identified only in P14SC. Additionally a larger number of genes were categorized to 'nervous system development and function', 'neurological disease', and 'psychological disorders' in P14SC than in E12IP.

ACKNOWLEDGMENT

This work was supported by Grants-in-Aid from the Food Safety Commission of Japan (No. 1003).

REFERENCES

Blackford, J.U. and Pine, D.S. (2012): Neural substrates of childhood anxiety disorders: a review of neuroimaging findings. Child Adolesc. Psychiatr. Clin. N. Am., **21**, 501-525.

Etkin, A. and Wager, T.D. (2007): Functional neuroimaging of anxiety: a meta-analysis of emotional processing in PTSD, social anxiety disorder, and specific phobia. Am. J. Psychiatry., **164**, 1476-1488.

Markram, K., Rinaldi, T., Mendola, D.L., Sandi, C. and Markram, H. (2008): Abnormal fear conditioning and amygdala processing in an animal model of autism. Neuropsychopharmacology, **33**, 901-912.

Neuhaus, E., Beauchaine, T.P. and Bernier, R. (2010): Neurobiological correlates of social functioning in autism. Clin. Psychol. Rev., **30**, 733-748.

Schneider, T. and Przewtocki, R. (2005): Behavioral alterations in rats prenatally exposed to valproic acid: Animal model of autism. Neuropsychopharmacology, **30**, 80-89.

Schneider, T., Ziolkowska, T., Gieryk, T., Tyminska, T. and Przewlocki, R. (2007): Prenatal exposure to valproic acid disturbs the enkephalinergic system functioning, basal hedonic tone, and emotional responses in an animal model of autism. Psychopharmacology, **193**, 547-555.

Schneider, T., Roman, A., Basta-Kaim, A., Kubera, M., Budziszewska, B., Schneider, K. and Przewtochi, R. (2008): Gender-specific behavioral and immunological alterations in an animal model of autism induced by prenatal exposure to valproic acid. Psychoneuroendocrinology, **33**, 728-740.

Wagner, G.C., Reuhl, K.R., Cheh, M., McRae, P. and Halladay, A.K. (2006): A new neurobehavioral model of autism in mice: Pre- and postnatal exposure to sodium valproate. J Autism Dev. Disord., **36**, 779-793.

Yochum, C.L., Dowling, P., Reuhl, K.R., Wagner, G.C. and Ming, X. (2008): VPA-induced apoptosis and behavioral deficits in neonatal mice. Brain Res., **1203**, 126-132.

Yochum, C.L., Bhattacharya, P., Patti, L., Mirochnitchenko, L. and Wagner, G.C. (2010): Animal model of autism using GSTM1 knockout mice and early post-natal sodium valproate treatment. Behav. Brain Res., **210**, 202-210.

Metallomics

RSC Publishing

PAPER

View Article Online
View Journal | View Issue

AMP-activated protein kinase-mediated glucose transport as a novel target of tributyltin in human embryonic carcinoma cells†

Cite this: *Metallomics*, 2013, 5, 484

Shigeru Yamada,[a] Yaichiro Kotake,[b] Yuko Sekino[a] and Yasunari Kanda*[a]

Received 28th December 2012,
Accepted 20th February 2013

DOI: 10.1039/c3mt20268b

www.rsc.org/metallomics

Organotin compounds such as tributyltin (TBT) are known to cause various forms of cytotoxicity, including developmental toxicity and neurotoxicity. However, the molecular target of the toxicity induced by nanomolar levels of TBT has not been identified. In the present study, we found that exposure to 100 nM TBT induced growth arrest in human pluripotent embryonic carcinoma cell line NT2/D1. Since glucose provides metabolic energy, we focused on the glycolytic system. We found that exposure to TBT reduced the levels of both glucose-6-phosphate and fructose-6-phosphate. To investigate the effect of TBT exposure on glycolysis, we examined glucose transporter (GLUT) activity. TBT exposure inhibited glucose uptake *via* a decrease in the level of cell surface-bound GLUT1. Furthermore, we examined the effect of AMP-activated protein kinase (AMPK), which is known to regulate glucose transport by facilitating GLUT translocation. Treatment with the potent AMPK activator, AICAR, restored the TBT-induced reduction in cell surface-bound GLUT1 and glucose uptake. In conclusion, these results suggest that exposure to nanomolar levels of TBT causes growth arrest by targeting glycolytic systems in human embryonic carcinoma cells. Thus, understanding the energy metabolism may provide new insights into the mechanisms of metal-induced cytotoxicity.

Introduction

Growing evidence suggests that environmental metals contribute to developmental toxicity and neurotoxicity.[1–3] Since the developing brain is inherently more vulnerable to injury than the adult brain, exposure to metals during early fetal development can potentially cause neurological disorders at doses much lower than those that are toxic in adults.[4–7] Therefore, it is necessary to elucidate the cytotoxic effects of such metals at low levels.

Organotin compounds are well known to cause cytotoxicity. Although organotin compounds or derivatives have been shown to have a potential anti-tumor activity[8,9] and some of them have already been entered into preclinical trials,[10] tributyltin (TBT) is considered to be associated with developmental toxicity and neurotoxicity.[11] For example, TBT can cause increased fetal mortality, decreased fetal birth weights, and behavioral abnormalities in rat offspring.[12,13] TBT is known to affect fertilization and embryonic development.[14] Moreover, TBT has been shown to induce neuronal death by glutamate excitotoxicity in cultured rat cortical neurons.[15] Although the use of TBT has already been restricted, butyltin compounds, including TBT, have been reported to be still present at concentrations between 50 and 400 nM in human blood.[16] However, the mechanism by which nanomolar levels of TBT cause cytotoxicity is not fully understood.

Glucose is the primary energy source for homeostasis. Glucose transport across the plasma membrane *via* a glucose transporter (GLUT) is a rate-limiting step in glucose metabolism.[17] AMP-activated protein kinase (AMPK), a serine threonine kinase, has been shown to regulate glucose uptake by facilitating the translocation of the GLUT to the membrane or by activation of transporter activity at the plasma membrane.[18,19] The fetal brain has been reported to rely on anaerobic glycolysis to meet its energy demands.[20] Thus, GLUT is considered essential in the early organogenesis period. GLUT1, a major subtype of GLUT in fetal tissue, has been shown to mediate organogenesis in rat embryos.[21] In addition, clinical data regarding human GLUT1 deficiency syndrome suggest that GLUT1 is necessary for human brain development.[22]

In the present study, we hypothesized a possible link between TBT toxicity and glucose metabolism. We found that

[a] *Division of Pharmacology, National Institute of Health Sciences, 1-18-1, Kamiyoga, Setagaya-ku 158-8501, Japan. E-mail: kanda@nihs.go.jp; Fax: +81-3-3700-9704; Tel: +81-3-3700-9704*

[b] *Department of Xenobiotic Metabolism and Molecular Toxicology, Graduate School of Biomedical and Health Sciences, Hiroshima University, Japan*

† Electronic supplementary information (ESI) available. See DOI: 10.1039/c3mt20268b

exposure to TBT reduced the amounts of glucose-6-phosphate and fructose-6-phosphate *via* a decrease in surface-bound GLUT1 in the human pluripotent embryonic carcinoma cell line NT2/D1. In addition, treatment with the potent AMPK activator, 5-aminoimidazole-4-carboxyamide ribonucleoside (AICAR), restored the inhibitory effect of TBT on both cell surface-bound GLUT1 levels and glucose uptake. We report here that the glycolytic pathway is a molecular target of nanomolar levels of TBT in human embryonic carcinoma cells.

Methods

Cell culture

NT2/D1 cells were obtained from the American Type Culture Collection. The cells were cultured in Dulbecco's modified Eagle's medium (DMEM; Sigma-Aldrich, St. Louis, MO, USA) supplemented with 10% fetal bovine serum (FBS; Biological Industries, Ashrat, Israel) and 0.05 mg mL^{-1} penicillin–streptomycin mixture (Life Technologies, Carlsbad, CA, USA) at 37 °C and 5% CO_2. For neural differentiation, all-trans retinoic acid (RA; Sigma-Aldrich) was added to the medium twice a week at a final concentration of 10 μM.

Cell proliferation assay

Cell viability was measured using the CellTiter 96 AQueous One Solution Cell Proliferation Assay (Promega, Madison, WI, USA), according to the manufacturer's instructions. Briefly, NT2/D1 cells were seeded into 96-well plates and exposed to different concentrations of TBT. After exposure to TBT, One Solution Reagent was added to each well, and the plate was incubated at 37 °C for another 2 h. Absorbance was measured at 490 nm using an iMark microplate reader (Bio-Rad, Hercules, CA, USA).

Glucose uptake assay

A glucose uptake assay was performed using a fluorescent glucose derivative, 2-[*N*-(7-nitrobenz-2-oxa-1,3-diazol-4-yl)amino]-2-deoxy-D-glucose (2-NBDG; Peptide Institute Inc., Osaka, Japan) by the previously reported procedure with slight modifications.[23] Briefly, NT2/D1 cells exposed to TBT were incubated with 2-NBDG (100 μM) for 2 h at 37 °C. The 2-NBDG uptake reaction was stopped by draining the incubation medium and washing the cells twice with ice-cold PBS. The incorporated 2-NBDG was measured using a Wallac1420ARVO fluoroscan (Perkin-Elmer, Waltham, MA, USA) with excitation at 488 nm and emission at 515 nm. The fluorescence intensities were normalized to the total protein content.

Hexokinase activity assay

Hexokinase activity was determined using a commercial Hexokinase Colorimetric Assay Kit (Biovision, Mountain View, CA, USA), according to the manufacturer's instructions.

AMPK activity assay

AMPK activity was determined using a commercial CycLex AMP Kinase Assay Kit (MBL International, Woburn, MA, USA), according to the manufacturer's instructions.

Determination of glucose-6-phosphate and fructose-6-phosphate

Intracellular metabolites were extracted and used for subsequent capillary electrophoresis time-of-flight mass spectrometry (CE-TOFMS) analysis, as described previously.[24] Glucose-6-phosphate and fructose-6-phosphate were determined using an Agilent CE capillary electrophoresis system (Agilent Technologies, Waldbronn, Germany) equipped with an Agilent G3250AA LC/MSD TOF system (Agilent Technologies, Palo Alto, CA), an Agilent 1100 series isocratic HPLC pump, a G1603A Agilent CE-MS adapter kit, and a G1607A Agilent CE-electrospray ionization 53-MS sprayer kit. For system control and data acquisition, G2201AA Agilent ChemStation software was used for CE, and Agilent TOF (Analyst QS) software was used for TOFMS.

Western blotting

Western blotting was performed as previously reported.[25] Briefly, the cells were lysed using Cell Lysis Buffer (Cell Signaling Technology, Danvers, MA, USA), and proteins were then separated by sodium dodecyl sulfate (SDS)-polyacrylamide gel electrophoresis and electrophoretically transferred to Immobilon-P membranes (Millipore, Billerica, MA, USA). The membranes were probed using primary antibodies (anti-GLUT1 polyclonal antibodies [1:200; Santa Cruz Biotechnology, Santa Cruz, CA, USA], anti-c-Myc polyclonal antibodies [1:1000; Sigma-Aldrich], anti-Flag monoclonal antibodies [1:1000; Sigma-Aldrich], and anti-β-actin monoclonal antibodies [1:1000; Sigma-Aldrich]). The membranes were then incubated with secondary antibodies against rabbit or mouse IgG conjugated with horseradish peroxidase (Cell Signaling Technology). The bands were visualized using an ECL Western Blotting Analysis System (GE Healthcare, Buckinghamshire, UK), and images were acquired using a LAS-3000 Imager (Fujifilm UK Ltd., Systems, Bedford, UK). The density of each band was quantified with ImageJ software (NIH, Bethesda, MD, USA).

Cell surface biotinylation

NT2/D1 cell surface proteins were biotinylated using a Cell Surface Protein Isolation Kit, according to the manufacturer's instructions (Pierce, Rockford, IL, USA). Briefly, cells were incubated with ice-cold phosphate-buffered saline (PBS; pH 7.4) containing Sulfo-NHS-SS-Biotin, with gentle rocking for 30 min at 4 °C. The biotinylated proteins were precipitated with streptavidin beads and eluted from the beads with SDS sample buffer. The proteins were analyzed by western blotting with anti-GLUT1 antibodies.

Immunohistochemistry

Cells, cultured on glass coverslips, were fixed in 4% paraformaldehyde in PBS (pH 7.4) for 15 min at room temperature. The fixed cells were incubated with anti-GLUT1 polyclonal antibodies (1:100; Santa Cruz) for 1 h at room temperature. Finally, they were incubated with Alexa488-conjugated secondary antibodies (1:200; Life Technologies) for 1 h at room temperature. The cells were enclosed in SlowFade (Life Technologies) and examined under a BIOREVO BZ-9000 fluorescent microscope (Keyence, Osaka, Japan).

Transfection

Cells were transiently transfected with Flag-tagged GLUT1 in pEF6 (a kind gift from Dr Rathmell) and c-Myc-tagged constitutively active-AMPK-α1 (T172D) or c-Myc-tagged dominant-negative-AMPK-α1 (K45R) in pcDNA3 (a kind gift from Dr Carling) using the FuGene HD Transfection Reagent (Promega), according to the manufacturer's protocol. After 48 h incubation, the transfectants were cultured with 12.5 μg mL^{-1} blasticidin or 0.5 mg mL^{-1} G418.

Real-time PCR

After total RNA was isolated from NT2/D1 cells using TRIzol (Life Technologies), quantitative real-time reverse transcription (RT)-PCR with a QuantiTect SYBR Green RT-PCR Kit (QIAGEN, Valencia, CA, USA) was performed using an ABI PRISM 7900HT sequence detection system (Applied Biosystems, Foster City, CA, USA), as previously reported.[26] The relative changes in the amounts of transcripts in each sample were normalized using ribosomal protein L13 (RPL13) mRNA levels. The sequences of the primers used for real-time PCR analysis are as follows: GLUT1 (forward, 5′-CCAGCTGCCATTGCCGTT-3′; reverse, 5′-GACGTAGGGACCACACAGTTGC-3′), GLUT2 (forward, 5′-CACACAAGACCTGGAATTGACA-3′; reverse, 5′-CGGTCATCCAGTGGAACAC-3′), GLUT3 (forward, 5′-CAATGCTCCTGAGAAGATCATAA-3′; reverse, 5′-AAAGCGGTTGACGAAGAGT-3′), GLUT4 (forward, 5′-CTGGGCCTCACAGTGCTAC-3′; reverse, 5′-GTCAGGCGCTTCAGACTCTT-3′), nestin (forward, 5′-GGCAGCGTTGGAACAGAGGT-3′; reverse, 5′-CATCTTGAGGTGCGCCAGCT-3′), NeuroD (forward, 5′-GGAAACGAACCCACTGTGCT-3′; reverse, 5′-GCCACACCAAATTCGTGGTG-3′), Math1 (forward, 5′-GTCCGAGCTGCTACAAACG-3′; reverse, 5′-GTGGTGGTGGTCGCTTTT-3′), MAP2 (forward, 5′-CCAATGGATTCCCATACAGG-3′; reverse, 5′-CTGCTACAGCCTCAGCAGTG-3′), RPL13 (forward, 5′-CATCGTGGCTAAACAGGTACTG-3′; reverse, 5′-GCACGACCTTGAGGGCAGCC-3′).

Materials

TBT was obtained from Tokyo Chemical Industry (Tokyo, Japan). Tin acetate (TA), AICAR, and rosiglitazone were obtained from Sigma-Aldrich. All other reagents were of analytical grade and obtained from commercial sources.

Statistical analysis

All data were presented as mean ± S.D. ANOVA followed by a *post hoc* Tukey test was used to analyze data in Fig. 1–4. Unpaired Student's *t* test was used to analyze data in Fig. 5. A *p* value of less than 0.05 was considered significant.

Results

To examine the effect of TBT on the proliferation of human NT2/D1 embryonic carcinoma cells, we exposed the cells to different concentrations of TBT for 24 h and measured cell viability by MTT assay. Treatment with TBT reduced cell viability in a dose-dependent manner (Fig. 1A; 0.03–0.3 μM). We observed that almost all cells were detached from the culture dish at TBT concentrations of 300 nM and above. In contrast, the less toxic TA had little effect at any concentration (Fig. 1A–e). We performed time-course experiments with 100 nM TBT, and determined the cell number. Exposure to

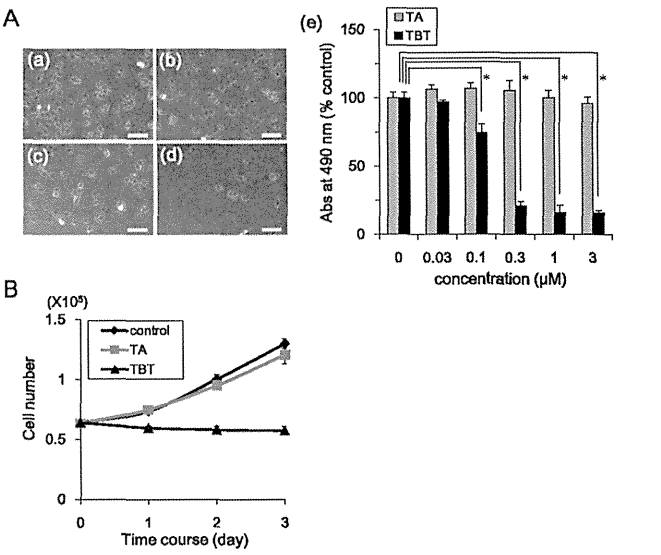

Fig. 1 Effect of TBT exposure on cell proliferation in NT2/D1 cells. (A) NT2/D1 cells were seeded into 96-well plates and exposed to TBT at different concentrations for 24 h. (a–d) Phase-contrast photomicrographs of NT2/D1 cells exposed to TBT at 0, 0.03, 0.1, or 0.3 μM (Bar = 100 μm). (e) Cell viability in the presence of TBT or TA was examined using the CellTiter 96 AQueous One Solution Cell Proliferation Assay. (B) NT2/D1 cells (6 × 10^5 cells) were seeded into 100 mm dishes and exposed to 100 nM TBT. After 24, 48, and 72 h, cell count was determined using a hemocytometer. *P < 0.05.

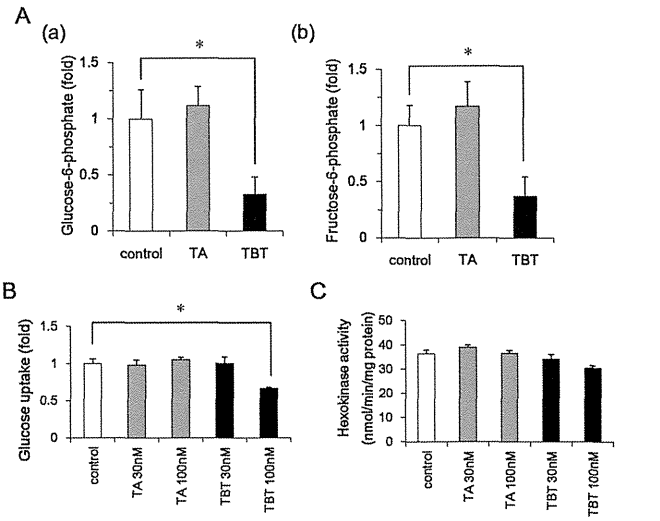

Fig. 2 Effect of TBT exposure on glycolytic systems in NT2/D1 cells. (A) After 24 h exposure to 100 nM TBT or TA, glucose 6-phosphate (a) and fructose 6-phosphate (b) levels were determined using CE-TOFMS. (B) After exposure to TBT or TA (30, 100 nM) for 24 h, glucose uptake assay was performed using a fluorescent glucose analog 2-NBDG. The fluorescence intensities of incorporated 2-NBDG were normalized to total cellular protein content. (C) After exposure to TBT or TA (30, 100 nM) for 24 h, hexokinase activity was measured using a commercial assay kit. *P < 0.05.

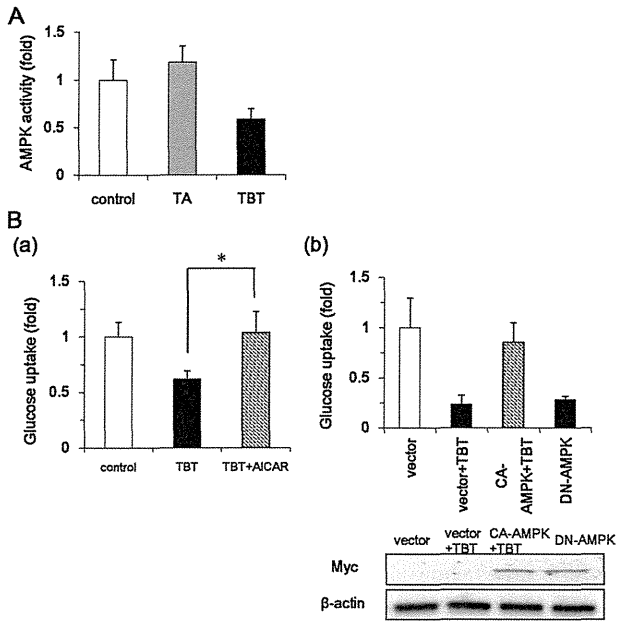

Fig. 3 Effect of AMPK on glucose uptake in NT2/D1 cells. (A) NT2/D1 cells were exposed to TBT or TA at 100 nM for 24 h. AICAR (0.5 mM) treatment was performed for 3 h. AMPK activity in the lysed cells was determined using a commercial assay kit. (B) NT2/D1 cells were exposed to TBT in the presence of 0.5 mM AICAR. (C) After overexpression of constitutively active (CA) mutants of AMPK, NT2/D1 cells were exposed to 100 nM TBT for 24 h, and glucose uptake assay was performed. After overexpression of dominant-negative (DN) mutants of AMPK, basal glucose uptake was tested. A glucose uptake assay was performed using the fluorescent glucose analog 2-NBDG. The fluorescence intensities of incorporated 2-NBDG were normalized to total cellular protein content. $^*P < 0.05$.

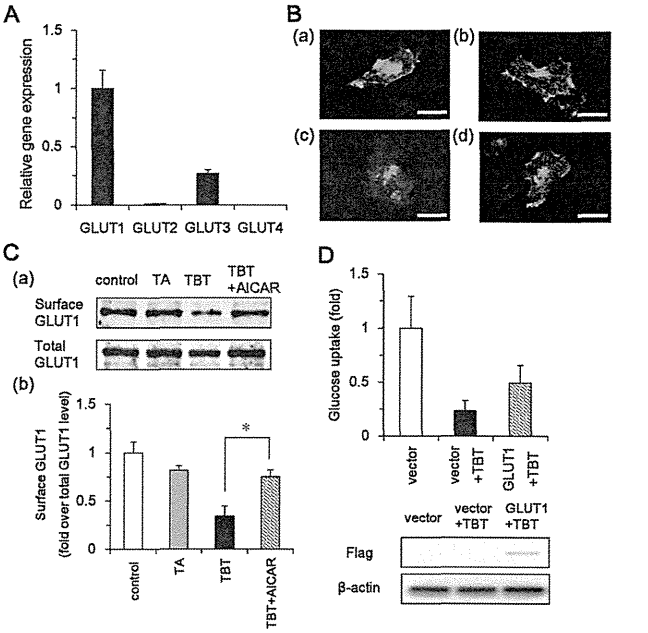

Fig. 4 Effect of TBT exposure on GLUT1 localization in NT2/D1 cells. (A) Expression of GLUT family by real-time PCR in NT2/D1 cells. Relative changes were determined by normalizing to RPL13. (B) After exposure to 100 nM TBT for 24 h, NT2/D1 cells were immunostained with anti-GLUT1 polyclonal antibodies. (a) Control, (b) 100 nM TA, (c) 100 nM TBT, and (d) 100 nM TBT + 0.5 mM AICAR. (Bar = 25 μm). (C) (a) NT2/D1 cell surface proteins were biotinylated using Sulfo-NHS-SS-Biotin, and then lysed. After precipitation with streptavidin beads, biotinylated proteins were analyzed by western blotting using anti-GLUT1 antibodies. Total GLUT1 protein was detected in cell lysate. (b) The relative density of bands was quantified with ImageJ software. Cell surface GLUT1 levels were normalized to total GLUT1 levels. (D) After overexpression of GLUT1, NT2/D1 cells were exposed to 100 nM TBT for 24 h, and glucose uptake assay was performed using the fluorescent glucose analog 2-NBDG. The fluorescence intensities of incorporated 2-NBDG were normalized to total cellular protein content. $^*P < 0.05$.

TBT suppressed the growth curve, but the total cell number did not alter throughout the time-course experiment (Fig. 1B). These data suggest that exposure to 100 nM TBT induced growth arrest in the cells without causing cell death.

Glucose provides metabolic energy for cell growth and it is incorporated by glucose transporters.[17] To examine the mechanism by which TBT induces growth arrest at low concentrations, we determined the glucose-6-phosphate, a major metabolite in glycolysis. We found that exposure to 100 nM TBT reduced the amount of glucose-6-phosphate (Fig. 2A). Fructose-6-phosphate, which is produced by isomerization of glucose 6-phosphate, also reduced by TBT. To check whether the decrease in glucose-6-phosphate is induced by inhibition of glucose transport, we examined the activity of glucose uptake by using 2-NBDG, a fluorescently labeled 2-deoxyglucose. Similar to the cell growth, glucose uptake was significantly inhibited by 100 nM TBT, not by 30 nM TBT (Fig. 2B). TA had little effect on glucose uptake. To examine whether the inhibition is regulated by transcription, we tested the effect of short-term exposure. Exposure to TBT for 1 h suppressed glucose uptake (Fig. S1, ESI†), suggesting that gene expression is not involved in the effect of TBT. Since TBT has been shown to activate transcriptional activity of peroxisome proliferator-activated receptor γ (PPARγ),[27,28] we tested the effect of the PPARγ agonist rosiglitazone on the glucose uptake. Treatment with rosiglitazone increased glucose uptake (Fig. S2, ESI†), suggesting that PPARγ is not involved in TBT-induced inhibition of glucose uptake. Furthermore, we examined the activity of hexokinase, which catalyzes the phosphorylation of glucose into glucose-6-phosphate. As shown in Fig. 2C, hexokinase activity was not significantly altered by TBT. Exposure to TA also produced similar results. These data suggest that TBT exposure decreases the amount of glycolytic metabolites *via* inhibition of glucose transport.

AMP-activated protein kinase (AMPK) is known to regulate the translocation of a glucose transporter (GLUT) to the plasma membrane.[29] We examined whether AMPK is involved in the inhibition of glycolytic systems by TBT exposure. Exposure to 100 nM TBT reduced AMPK activity (Fig. 3A). In contrast, TA had little effect on AMPK. In addition, treatment with AICAR (a potent AMPK activator) recovered the inhibitory effect of TBT on glucose uptake (Fig. 3B). To confirm the effect of AICAR, we examined the effect of constitutively active (CA) mutants of AMPK. Similar to the treatment with AICAR, overexpression of CA-AMPK recovered the inhibitory effect of TBT on glucose uptake. Overexpression of dominant-negative mutants of AMPK reduced the basal level of glucose uptake, suggesting that

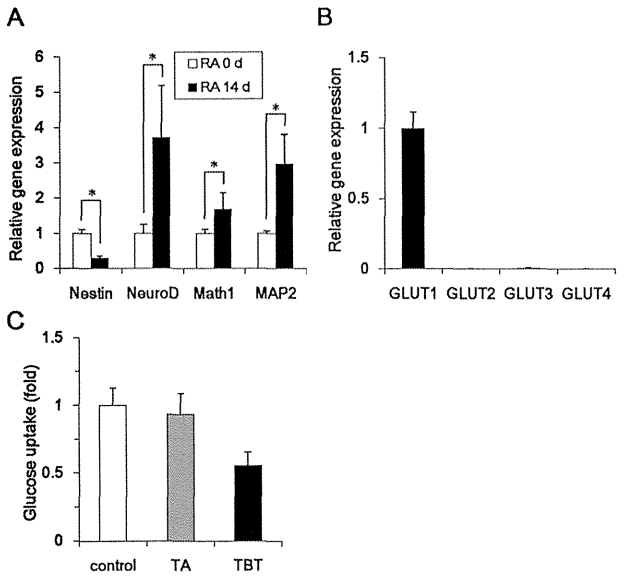

Fig. 5 Effect of neuronal induction on glucose uptake under TBT exposure in NT2/D1 cells. (A) To induce neuronal differentiation, NT2/D1 cells were treated with 10 μM RA for 14 days. The relative expression of neuronal markers (NeuroD, Math1, and MAP2) and a marker of undifferentiation (nestin) were measured by real-time-PCR. The relative changes were normalized to RPL13. (B) Expressions of members of the GLUT family were measured by real-time PCR in differentiated NT2/D1 cells. Relative changes were determined by normalizing to RPL13. (C) After exposure to 100 nM TBT for 24 h, glucose uptake was measured in differentiated cells. The fluorescence intensities of intracellularly incorporated 2-NBDG were measured and normalized to the total cellular protein levels. $^*P < 0.05$.

glucose uptake is AMPK-dependent in NT2/D1 cells. Taken together, these data suggest that TBT exposure suppresses glucose uptake through the inhibition of AMPK activity.

We next examined the mechanism by which AMPK regulates glucose uptake in NT2/D1 cells. Real-time PCR analysis showed that GLUT1 was a major subtype in NT2/D1 cells (Fig. 4A). Since TBT exposure did not affect gene expression of GLUT1 (data not shown), we examined GLUT1 localization by immunohistochemistry. Expression of GLUT1 was observed at the plasma membrane and in the intracellular segment (Fig. 4B). Exposure with TBT reduced the cell surface expression of GLUT1. Treatment with AICAR recovered the inhibitory effect of TBT. To confirm these observations using microscopy, we labeled cell surface-bound GLUT1 by biotinylation of cell surface proteins (Fig. 4C). Using this approach, we determined that TBT exposure reduced the amount of cell surface-bound GLUT1. AICAR reversed this inhibitory effect of TBT. Furthermore, overexpression of GLUT1 partially recovered the TBT-induced inhibition of glucose uptake (Fig. 4D). These data suggest that TBT inhibits glucose uptake mediated by cell surface translocation of GLUT1, a process dependent on AMPK.

To examine whether the effect of TBT was selective for embryonic cells, we used NT2/D1 cells differentiated by retinoic acid.[30] Real-time PCR analysis revealed that RA-treated NT2/D1 cells showed upregulated expression of markers of differentiation (NeuroD, Math1, MAP2) and downregulated expression of a marker of undifferentiation (nestin), confirming the induction of differentiation (Fig. 5A). Real-time PCR confirmed that GLUT1 is a major subtype in the differentiated NT2/D1 cells (Fig. 5B). Furthermore, exposure to 100 nM TBT also reduced glucose uptake in differentiated NT2/D1 cells. In contrast, TA had little effect (Fig. 5C). These data suggest that TBT suppresses glucose uptake in both undifferentiated and differentiated cells.

Discussion

In the present study, we showed that the glycolytic pathway is a novel target of TBT toxicity in human embryonic carcinoma cells. We showed that TBT suppresses AMPK-dependent glucose uptake, and thereby, the amount of glucose-6-phosphate. The inhibitory effects of TBT on glycolytic systems would lead to growth arrest in the cells. Fig. 6 shows a proposed model of TBT-induced toxicity, based on the data observed in our study.

Our studies showed that treatment with 1 μM TBT resulted in the death of human embryonic carcinoma cells (Fig. 1). Consistent with these observations, previous studies have shown that micromolar levels of TBT induce apoptosis in various cells such as human amnion cells,[31] hepatocytes,[32] and neutrophils.[33] In contrast, exposure to 100 nM TBT resulted in neither growth arrest nor cell death. Therefore, we focused on intracellular metabolites as potential mediators of TBT-induced growth arrest. We found that exposure to nanomolar levels of TBT affects the intracellular metabolic balance and decreases the amount of glucose metabolites (Fig. 2). A previous report showed that the organotin compounds such as TBT might be present in human blood at nanomolar levels.[16] Glucose metabolism analysis revealed novel toxic mechanisms

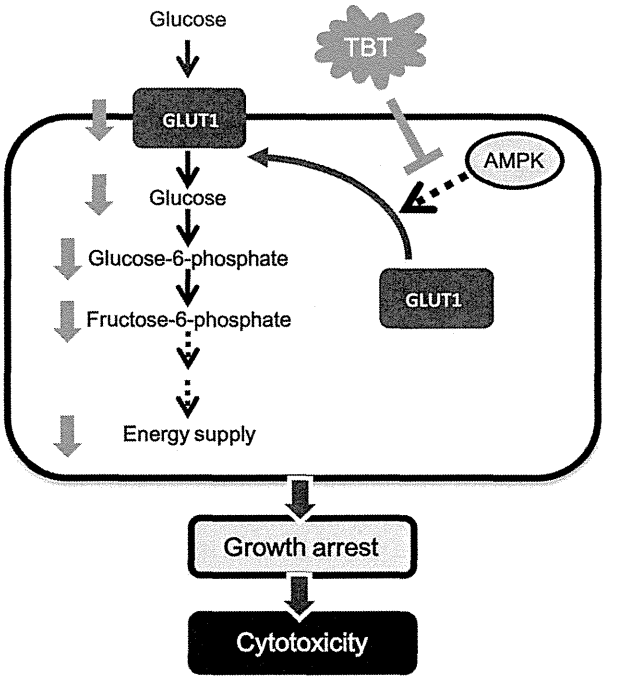

Fig. 6 Proposed model of TBT toxicity in human embryonic carcinoma cells.

for the toxicity of nanomolar levels of TBT. Thus, the glycolytic pathway might account for the unknown toxic mechanism induced by heavy metal exposure.

Our data suggest that the target molecule of TBT toxicity is GLUT1, a major subtype of GLUT in NT2/D1 cells (Fig. 4). Since the expression of GLUT1 is observed in a broad range of cell types, the toxicity of TBT may also be observed in other cells. For example, we showed that TBT reduces glucose uptake in differentiated NT2/D1 cells, which express GLUT1 (Fig. 5). Thus, it is possible that TBT induces toxicity in mature neurons *via* inhibition of GLUT function.

We showed that TBT decreases AMPK activity, one of the GLUT regulators, in NT2/D1 cells (Fig. 3). In addition, overexpression of AMPK or the AMPK activator restored the glucose uptake, confirming that AMPK is a possible target of TBT. In contrast, 500 nM TBT has been shown to increase AMPK phosphorylation in rat cortical neurons.[34] This discrepancy might be due to the concentration of TBT or different types of cells.

Several studies suggest that TBT directly interacts with target enzymes. TBT at a concentration of 10–100 nM has been shown to act as an agonist of PPARγ and the retinoid X receptor (RXR) because of its higher binding affinity compared to intrinsic ligands. Other studies reported that micromolar concentrations of TBT inhibit F1F0 ATP synthase and 11β-hydroxysteroid dehydrogenase by direct interaction.[35,36] Therefore, TBT can bind to multiple targets with broad specificity. It is possible that TBT also interacts with AMPK. On the other hand, calmodulin-dependent protein kinase II (CaMK II) and serine–threonine liver kinase B1 (LKB1) have been shown to phosphorylate AMPK and cause subsequent activation of glucose transport.[29] Furthermore, there may be an additional signaling molecule between TBT and AMPK. It remains to be elucidated how TBT regulates AMPK in embryonic carcinoma cells.

Nanomolar levels of TBT may interact with several targets in other types of cells, such as PPARγ, RXR, and α-amino-3-hydroxy-5-methylisoxazole-4-propionic acid (AMPA) receptors 2 (GluR2). Since rosiglitazone, a PPARγ agonist, increased glucose transport in NT2/D1 cells (Fig. S2, ESI†), it is unlikely that TBT inhibits glucose transport *via* PPARγ in the cells. RXR transgenic mice have been shown to exhibit an increase in GLUT1 expression in the skeletal muscles.[37] Since the expression level of GLUT1 was not changed by TBT exposure in NT2/D1 cells and the inhibitory effect of glucose uptake was observed after a 1 h treatment with TBT, it is likely that RXR is not involved in TBT-mediated alteration of glucose transport. Moreover, exposure to nanomolar levels of TBT has been reported to decrease the mRNA expression of GluR2 in cultured rat cortical neurons.[38] Although NT2/D1 cells do not express GluR2, it is possible that GluR2 may be a target in the differentiated NT2/D1 cells. Further studies are required to examine these targets other than the glycolytic pathway.

Conclusions

We found that exposure to nanomolar levels of TBT mainly targets the glycolytic systems in human embryonic carcinoma cells. Thus, glycolytic systems may be a good target for previously unknown mechanisms of toxicity induced by metal exposure at nanomolar levels.

Conflict of interest

The authors declare that there are no conflicts of interest.

List of abbreviations

AMPK	AMP-activated protein kinase
GLUT	glucose transporter
RA	all-trans retinoic acid
PPARγ	peroxisome proliferator-activated receptor γ
TA	tin acetate
TBT	tributyltin

Acknowledgements

We would like to thank Dr Rathmell and Dr Carling for providing the materials. This study was supported in part by a Health and Labour Sciences Research Grant from the Ministry of Health, Labour and Welfare, Japan (Y. Ka.), a grant from the Program for Promotion of Fundamental Studies in Health Sciences of the National Institute of Biomedical Innovation (NIBIO) (No. 09-02 to Y. Ka.), Grants-in-Aid for Scientific Research (No. 23590322 to Y. Ka. and No. 23310047 to Y. Ko.) from the Japan Society for the Promotion of Science, and a grant from the Smoking Research Foundation (Y. Ka.).

References

1 H. L. Needleman, C. Gunnoe, A. Leviton, R. Reed, H. Peresie, C. Maher and P. Barrett, Deficits in psychologic and classroom performance of children with elevated dentine lead levels, *N. Engl. J. Med.*, 1979, **300**, 689–695.
2 G. Winneke, Developmental aspects of environmental neurotoxicology: lessons from lead and polychlorinated biphenyls, *J. Neurol. Sci.*, 2011, **308**, 9–15.
3 L. G. Costa, M. Aschne, A. Vitalone, T. Syversen and O. P. Soldin, Developmental neuropathology of environmental agents, *Annu. Rev. Pharmacol. Toxicol.*, 2004, **44**, 87–110.
4 J. Dobbing, *Vulnerable periods in developing brain*, in *Appl. Neurochem.*, ed. A. N. Davison and J. Dobbing, Davis, Philadelphia, 1968, pp. 287–316.
5 P. M. Rodier, Developing brain as a target of toxicity, *Environ. Health Perspect.*, 1995, **103**(suppl 6), 73–76.
6 D. Rice and S. Barone Jr, Critical periods of vulnerability for the developing nervous system: evidence from humans and animal models, *Environ. Health Perspect.*, 2000, **108**(suppl 3), 511–533.
7 H. Asakawa, M. Tsunoda, T. Kaido, M. Hosokawa, C. Sugaya, Y. Inoue, Y. Kudo, T. Satoh, H. Katagiri, H. Akita, M. Saji, M. Wakasa, T. Negishi, T. Tashiro and Y. Aizawa, Enhanced

inhibitory effects of TBT chloride on the development of F1 rats, *Arch. Environ. Contam. Toxicol.*, 2010, **58**, 1065–1073.
8 S. Gómez-Ruiz, G. N. Kaluderović, S. Prashar, E. Hey-Hawkins, A. Erić, Z. Zizak and Z. D. Juranić, Study of the cytotoxic activity of di and triphenyltin(IV) carboxylate complexes, *J. Inorg. Biochem.*, 2008, **102**, 2087–2096.
9 L. Rocamora-Reverte, E. Carrasco-García, J. Ceballos-Torres, S. Prashar, G. N. Kaluđerović, J. A. Ferragut and S. Gómez-Ruiz, Study of the anticancer properties of tin(IV) carboxylate complexes on a panel of human tumor cell lines, *ChemMedChem*, 2012, 7, 301–310.
10 A. González, E. Gómez, A. Cortés-Lozada, S. Hernández, T. Ramírez-Apan and A. Nieto-Camacho, Heptacoordinate tin(IV) compounds derived from pyridine Schiff bases: synthesis, characterization, *in vitro* cytotoxicity, anti-inflammatory and antioxidant activity, *Chem. Pharm. Bull.*, 2009, **57**, 5–15.
11 Y. Kotake, Molecular mechanisms of environmental organotin toxicity in mammals, *Biol. Pharm. Bull.*, 2012, **35**, 1876–1880.
12 T. Noda, S. Morita, T. Yamano, M. Shimizu, T. Nakamura, M. Saitoh and A. Yamada, Teratogenicity study of tri-*n*-butyltin acetate in rats by oral administration, *Toxicol. Lett.*, 1991, **55**, 109–115.
13 A. T. Gardlund, T. Archer, K. Danielsen, B. Danielsson, A. Frederiksson, N. G. Lindquist, H. Lindstrom and J. Luthman, Effects of prenatal exposure to tributyltin and trihexyltin on behavior in rats, *Neurotoxicol. Teratol.*, 1991, **13**, 99–105.
14 Q. Li, M. Osada, K. Takahashi, T. Matsutani and K. Mori, Accumulation and depuration of tributyltin oxide and its effect on the fertilization and embryonic development in the pacific oyster, *Crassostrea gigas*, *Bull. Environ. Contam. Toxicol.*, 1997, **58**, 489–496.
15 Y. Nakatsu, Y. Kotake, K. Komasaka, H. Hakozaki, R. Taguchi, T. Kume, A. Akaike and S. Ohta, Glutamate excitotoxicity is involved in cell death caused by tributyltin in cultured rat cortical neurons, *Toxicol. Sci.*, 2006, **89**, 235–242.
16 M. M. Whalen, B. G. Loganathan and K. Kannan, Immunotoxicity of environmentally relevant concentrations of butyltins on human natural killer cells *in vitro*, *Environ. Res. Lett.*, 1999, **81**, 108–116.
17 L. Pellerin, Food for thought: the importance of glucose and other energy substrates for sustaining brain function under varying levels of activity, *Diabetes Metab.*, 2010, **36**, S59–S63.
18 K. Barnes, J. C. Ingram, O. H. Porras, L. F. Barros, E. R. Hudson, L. G. Fryer, F. Foufelle, D. Carling, D. G. Hardie and S. A. Baldwin, Activation of GLUT1 by metabolic and osmotic stress: potential involvement of AMP-activated protein kinase (AMPK), *J. Cell Sci.*, 2002, **115**, 2433–2442.
19 M. Jing, V. K. Cheruvu and F. Ismail-Beigi, Stimulation of glucose transport in response to activation of distinct AMPK signaling pathways, *Am. J. Physiol.: Cell Physiol.*, 2008, **295**, C1071–C1082.
20 B. Kunievsky, J. Pretsky and E. Yavin, Transient rise of glucose uptake in the fetal rat brain after brief episodes of intrauterine ischemia, *Dev. Neurosci.*, 1994, **16**, 313–320.
21 K. Matsumoto, S. Akazawa, M. Ishibashi, R. A. Trocino, H. Matsuo, H. Yamasaki, Y. Yamaguchi, S. Nagamatsu and S. Nagataki, Abundant expression of GLUT1 and GLUT3 in rat embryo during the early organogenesis period, *Biochem. Biophys. Res. Commun.*, 1995, **209**, 95–102.
22 P. J. Jensen, J. D. Gitlin and M. O. Carayannopoulos, GLUT1 deficiency links nutrient availability and apoptosis during embryonic development, *J. Biol. Chem.*, 2006, **281**, 13382–13387.
23 Y. Kanda and Y. Watanabe, Thrombin-induced glucose transport *via* Src-p38 MAPK pathway in vascular smooth muscle cells, *Br. J. Pharmacol.*, 2005, **146**, 60–67.
24 T. Soga, Y. Ueno, H. Naraoka, Y. Ohashi, M. Tomita and T. Nishioka, Simultaneous determination of anionic intermediates for *Bacillus subtilis* metabolic pathways by capillary electrophoresis electrospray ionization mass spectrometry, *Anal. Chem.*, 2002, **74**, 2233–2239.
25 Y. Kanda and Y. Watanabe, Adrenaline increases glucose transport *via* a Rap1-p38MAPK pathway in rat vascular smooth muscle cells, *Br. J. Pharmacol.*, 2007, **151**, 476–482.
26 N. Hiarta, Y. Sekinoa and Y. Kanda, Nicotine increases cancer stem cell population in MCF-7 cells, *Biochem. Biophys. Res. Commun.*, 2010, **403**, 138–143.
27 T. Kanayama, N. Kobayashi, S. Mamiya, T. Nakanishi and J. Nishikawa, Organotin compounds promote adipocyte differentiation as agonists of the peroxisome proliferator-activated receptor gamma/retinoid X receptor pathway, *Mol. Pharmacol.*, 2005, **67**, 766–774.
28 F. Grün, H. Watanabe, Z. Zamanian, L. Maeda, K. Arima, R. Cubacha, D. M. Gardiner, J. Kanno, T. Iguchi and B. Blumberg, Endocrine-disrupting organotin compounds are potent inducers of adipogenesis in vertebrates, *Mol. Endocrinol.*, 2006, **20**, 2141–2155.
29 D. G. Hardie, F. A. Ross and S. A. Hawley, AMPK: a nutrient and energy sensor that maintains energy homeostasis, *Nat. Rev. Mol. Cell Biol.*, 2012, **13**, 251–262.
30 S. J. Pleasure, C. Page and V. M. Lee, Pure, postmitotic, polarized human neurons derived from NTera 2 cells provide a system for expressing exogenous proteins in terminally differentiated neurons, *J. Neurosci.*, 1992, **12**, 1802–1815.
31 X. Zhu, M. Xing, J. Lou, X. Wang, W. Fu and L. Xu, Apoptotic related biochemical changes in human amnion cells induced by tributyltin, *Toxicology*, 2007, **230**, 45–52.
32 M. Grondin, M. Marion, F. Denizeau and D. A. Averill-Bate, Tributyltin induces apoptotic signaling in hepatocytes through pathways involving the endoplasmic reticulum and mitochondria, *Toxicol. Appl. Pharmacol.*, 2007, **222**, 57–68.
33 V. Lavastre and D. Girard, Tributyltin induces human neutrophil apoptosis and selective degradation of cytoskeletal proteins by caspases, *J. Toxicol. Environ. Health, Part A*, 2002, **65**, 1013–1024.

34 Y. Nakatsu, Y. Kotake, A. Hino and S. Ohta, Activation of AMP-activated protein kinase by tributyltin induces neuronal cell death, *Toxicol. Appl. Pharmacol.*, 2008, **230**, 358–363.
35 C. von Ballmoos, J. Brunner and P. Dimroth, The ion channel of F-ATP synthase is the target of toxic organotin compounds, *Proc. Natl. Acad. Sci. U. S. A.*, 2004, **101**, 11239–11244.
36 A. G. Atanasov, L. G. Nashev, S. Tam, M. E. Baker and A. Odermatt, Organotins disrupt the 11β-hydroxysteroid dehydrogenase type 2-dependent local inactivation of glucocorticoids, *Environ. Health Perspect.*, 2005, **113**, 1600–1606.
37 S. Sugita, Y. Kamei, F. Akaike, T. Suganami, S. Kanai, M. Hattori, Y. Manabe, N. Fujii, T. Takai-Igarashi, M. Tadaishi, J. Oka, H. Aburatani, T. Yamada, H. Katagiri, S. Kakehi, Y. Tamura, H. Kubo, K. N. S. Miura, O. Ezaki and Y. Ogawa, Increased systemic glucose tolerance with increased muscle glucose uptake in transgenic mice overexpressing RXRγ in skeletal muscle, *PLoS One*, **6**, e20467.
38 Y. Nakatsu, Y. Kotake Y, T. Takishit and S. Ohta, Long-term exposure to endogenous levels of tributyltin decreases GluR2 expression and increases neuronal vulnerability to glutamate, *Toxicol. Appl. Pharmacol.*, 2009, **240**, 292–298.